Electromagnetic Coupling and Radiation Loss Considerations in Microstrip (M)MIC Design

First Semi-annual Report

W. P. Harokopus, Jr. and P. B. Katehi
The Radiation Laboratory
Electrical Engineering and Computer Science Department
1301 Beal Ave.
University of Michigan, Ann Arbor MI., 48109

April, 1990

363707-1-T = RL-2535

Abstract-The high frequency characterization of microstrip meander lines, junctions, and stubs has been performed by the application of the method of moments to the electric field integral equation. Electromagnetic coupling, radiation, and substrate effects are inherently included with the use of the space domain Green's function. Conductor loss is also included by replacing the conductive strips with appropriate surface impedance boundaries.

List of Figures

1 Introduction

Fullwave Analysis has been successfully applied to a wide variety of microstrip discontinuities and components [1]-[6]. These techniques, accounting for electromagnetic coupling, radiation, and substrate effects, are important in high frequency circuit optimization. The analysis applied in this paper[6] has previously shown excellent accuracy in the high-frequency characterization of a variety of microstrip structures. Although not a substitute for less intensive approximate techniques (eg. quasi-static[7]-[11] and dispersive[12]-[15]), this method has proven to be versatile for microstrip characterization in regions where these techniques fail. The aim of this paper is to characterize commonly used microstrip elements in an effort to establish useful design guidelines. In the following sections, results for microstrip meander lines, transmission line junctions, and tuning stubs are presented.

The utilization of the meander line as a phase shifter or slow-wave structure in (M)MIC's is commonplace. Perhaps less well known is the usefulness of meander lines as narrowband filters. Examples will be given that demonstrate the effect of coupling on the slow-wave nature of the line, and quantify return loss, radiation, and conductor loss for a phase shifting section. Also, a meander line having a pencil thin passband will be shown.

Transmission line junctions are the most commonly used microstrip structures in (M)MICS. Often, their non-ideal effects may be neglected. Nevertheless, radiation loss can become significant in bend and T-junction discontinuities at high frequencies. Furthermore, tapering or mitering of junctions is often done to reduce return loss, but the corresponding effect on radiation is not known. Results on

radiation loss will be presented for right-angle and mitered bends, and multi-port tee and cross junctions.

The last class of structures presented in this paper are tuning stubs, which are frequently used in matching networks of (M)MIC amplifiers and oscillators. In the design of input matching stages for amplifiers, there exists a keen interest in the reduction of radiation loss, which in turn will improve noise performance. Several stub geometries will be presented, and an evaluation will be conducted of their respective bandwidths and radiation losses. Furthermore, a matching circuit for a 94 GHz oscillator will be examined to illustrate the effect spurious coupling and radiation loss have on performance.

2 Theory

Cross-sectional and top-views of the microstrip structure are shown in figure 1. The conductors are lossless and their thickness (t) is much smaller than a wavelength. The substrate is of thickness h, and is also assumed lossless. The electric field may be written in terms of an integral equation

$$\bar{E}(x,y,z) = \int\int_{S'} [k_i^2 \bar{\bar{I}} + \bar{\bar{\nabla}}\bar{\bar{\nabla}}]\bar{\bar{G}}(x,y,z/x',y',z') \cdot \bar{J}(x',y')ds' \quad i = 0,1 \qquad (1)$$

with k_0 and k_1 being the wave numbers in the free-space and dielectric regions respectively, and where

$$\bar{J}(x',y') = J_x(x',y')\hat{x} + J_y(x',y')\hat{y} \qquad (2)$$

is the current on the microstrip conducting strips. The components of the dyadic Green's function [17]

$$\bar{\bar{G}}(x,y,z/x',y',z') = G_{xx}\hat{x}\hat{x} + G_{zx}\hat{z}\hat{x} + G_{yy}\hat{y}\hat{y} + G_{zy}\hat{z}\hat{y} \tag{3}$$

are expressed in the form of Sommerfeld integrals

$$G_{xx} = G_{yy} = -\frac{j\omega\mu_0}{2\pi k_0^2}\int_0^\infty J_0(\lambda\rho)u_0\frac{e^{-u_0 z}\sinh uh}{f_1(\lambda,\epsilon_{r1},h)}\lambda d\lambda \qquad Z > 0 \tag{4}$$

$$G_{zx} = \tan(\phi)G_{zy} = -\frac{j\omega\mu_0}{2\pi k_0^2}(1-\epsilon_r)\cos\phi\int_0^\infty J_1(\lambda\rho)\frac{e^{-u_0 z}\sinh uh\cosh uh}{f_1(\lambda,\epsilon_{r1},h)f_2(\lambda,\epsilon_{r1},h)}\lambda^2 d\lambda \tag{5}$$

$$G_{xx} = G_{yy} = -\frac{j\omega\mu_0}{4\pi k^2}\int_0^\infty J_0(\lambda\rho)\frac{\sinh u(z+h)}{f_1(\lambda,\epsilon_{r1},h)}\lambda d\lambda \qquad Z < 0 \tag{6}$$

$$G_{zx} = \tan(\phi)G_{zy} = -\frac{j\omega\mu_0}{4\pi k^2}(1-\epsilon_r)\cos\phi\int_0^\infty J_1(\lambda\rho)\frac{\sinh uh\cosh u(z+h)}{f_1(\lambda,\epsilon_{r1},h)f_2(\lambda,\epsilon_{r1},h)}\lambda^2 d\lambda \tag{7}$$

with $\rho = \sqrt{(x-x')^2+(y-y')^2}$, $u_0 = \sqrt{\lambda^2 - k_0^2}$, and $u = \sqrt{\lambda^2 - k_1^2}$. The zeroes of the functions $f_1(\lambda,\epsilon_{r1},h)$ and $f_2(\lambda,\epsilon_{r1},h)$, given by

$$f_1(\lambda,\epsilon_{r1},h) = u_0\sinh uh + u\cosh uh \tag{8}$$

$$f_2(\lambda,\epsilon_{r1},h) = \epsilon_r u_0\sinh uh + u\cosh uh \tag{9}$$

represent the excited surface wave modes. In equations (8) and (9), ϵ_r is the relative dielectric constant, and h is the thickness of the substrate.

Resistive losses may also be included by the replacement of the conductive strips with impedance boundaries. The boundary conditions on the strip conductors are imposed through the following relation

$$\bar{E}_t(x,y,z=t) = \bar{\bar{Z}}\cdot(\bar{H}\times\hat{z}) \qquad x,y \in S \tag{10}$$

where $\bar{E}_t$ is the tangential electric field over the surface (S) of the conducting strips and

$$\bar{\bar{Z}}(f) = z_x\hat{x}\hat{x} + z_y\hat{y}\hat{y} \tag{11}$$

represents the appropriate surface impedance boundaries. The magnetic field is related to current on the strip conductor by the expression

$$\hat{z} \times \bar{H} = \bar{J}(x', y') \quad . \tag{12}$$

In view of equation (12), equation (1) takes the form

$$\int\int_{S'} [k_0^2 \bar{\bar{I}} + \bar{\bar{\nabla}}\bar{\bar{\nabla}}] \bar{\bar{G}}(x, y, z/x', y', z') \cdot \bar{J}(x', y') ds' + \bar{\bar{Z}} \cdot \bar{J}(x', y') = 0 \tag{13}$$

At microwave frequencies, radiation from discontinuities introduces losses which dominate the conductor losses unless long line lengths are present [19].[20]. In this work, the formulation will account for conductor loss in the meander delay line example. In all other examples perfect conductors will be considered ($\bar{E}_t(x, y, z = t) = 0$).

The microstrip discontinuity is subdivided into squares, and the method of moments is applied with roof-top basis functions. The unknown current is expressed in the form of double summations shown below

$$J_x = \sum_{n=1}^{N+1} \sum_{m=1}^{M+1} I_{nm}^x j_{nm}^x(x', y') \tag{14}$$

$$J_y = \sum_{n=1}^{N+1} \sum_{m=1}^{M+1} I_{nm}^y j_{nm}^y(x', y') \tag{15}$$

where

$$j_{nm}^x(x', y') = [f_n(x') g_m(y')] \tag{16}$$

$$j_{nm}^y(x', y') = [g_n(x') f_m(y')] \tag{17}$$

In equations (14) and (15), I_{nm} is the unknown current amplitude at the $(n, m)^{th}$ position of the subdivided element. The functions f_n and g_m are sub-domain shaping or basis functions and are consistent with the current boundary conditions.

The roof-top sub-domain basis functions have piecewise sinusoidal variation in the longitudinal direction and constant variation in the transverse direction according to

$$f_n(x') = \begin{cases} \frac{\sin k_s(x_{n+1}-x')}{\sin k_s l_x} & x_n \le x' \le x_{n+1} \\ \frac{\sin k_s(x'-x_{n-1})}{\sin k_s l_x} & x_{n-1} \le x' \le x_n \\ 0 & Else \end{cases} \tag{18}$$

and

$$g_m(y') = \begin{cases} 1 & y_m \le y' \le y_{m+1} \\ 0 & Else \end{cases} \tag{19}$$

In the above, $l_x = x_{n+1} - x_n$, and k_s is a scaling parameter chosen to vary between k_0 (free space wavenumber) and k_1 (wavenumber in the dielectric).

Substitution of the above into the electric field integral equation (equation 1) and application of Galerkin's method results in the matrix equation

$$\left[Z \right] \left[I \right] = \left[V \right]$$

where Z is the impedance matrix, I is the vector of unknown x and y current amplitudes, and V is the excitation vector, which is identically zero everywhere except at points where sources are located. In order to excite the discontinuity, voltage gap generators are utilized. The presence of the infinitesimally small gap is reflected in the excitation vector where

$$V_x^{\nu\mu} = \begin{cases} 1 & if \quad x_\nu = x_g \\ 0 & Else \end{cases} \tag{20}$$

and

$$V_y^{\nu\mu} = \begin{cases} 1 & if \quad y_\mu = y_g \\ 0 & Else \end{cases} \tag{21}$$

When a single microstrip mode is excited along the feeding line, the current forms TEM-like standing waves. Under this assumption, the microstrip element may be represented as an N-port network with the port voltages and currents related according to

$$V_n = \sum_{m=1}^{N} Z_{nm} I_m \qquad \forall n \in (1, N) \tag{22}$$

Dividing each voltage V_n by the corresponding current I_n results in the following expression for the input impedance Zin_n at port n.

$$Zin_n = \sum_{m=1}^{N} Z_{nm} (\frac{I_m}{I_n}) \tag{23}$$

The input impedances Zin_n, and reflection coefficients Γ_n, (n=1,N) are determined at a given reference plane from the method of moments current solution. An N-port discontinuity has N^2 unknown network parameters. This number can be reduced with reciprocity and symmetry as done in previous work, but in general, N^2 independent equations are required. These may be obtained from (22) after exciting the N-port microstrip element by N independent excitations.

3 Meander Lines

Meander lines are often used in (M)MICS as delay or slow wave lines, and also in monolithic antenna arrays for the phasing of the radiating elements as shown in Figure 2. In this application, a two layer structure is shown with an embedded

meander line feeding the antenna elements on the top of the substrate. Such a feed structure is also capable of exciting a slot array. The ability to adjust the spacing (S), the depth (d), the period length (L_p), and the number of periods(N) provides flexibility in the phasing of the radiating elements. Therefore, meander lines are particularly suited for use in beam forming and steering[23]. Successful design of such structures requires accurate models, which include the presence of bend discontinuities and the effect of electromagnetic coupling. Radiation and conductor loss may also have significant effects. Figure 3 presents the transmission parameter as a function of line length for a meander line on a 20 mil duroid substrate ($\epsilon_r = 2.2$) at 20 GHz. Two cases are shown: 1) with both resistive and radiation loss, and 2) radiation loss only. In this example, the substrate is electrically thin and radiation loss is not large. Conductor loss is essentially the difference between the two curves, and increases steadily with line length. This example illustrates an interesting point concerning the relative importance of radiation and resistive losses. Radiation losses in microstrip circuits are associated with fringing fields present at discontinuities, and are minimized through the reduction of the number of discontinuites, the use of electrically thin substrates, and through creative designs to be discussed further in the following sections. Resistive loss depends on the composition and shape of conductors, and increases with line length. For the following examples, where discontinuites are considered with relatively short lengths of line, only radiation loss will be included.

The unit phase delay (Pd_1) can be defined as the phase shift (Pd) of the line divided by the number of periods (N). To demonstrate the effect that the cascading

of several sections has on the phase, a meander delay line on a 25 mil alumina substrate has been analyzed. In Figure 4, the unit phase delay is shown as a function of frequency for cascades of 1, 2 and 3 periods, respectively. As shown, the unit phase delay is independent of the length of the line from 5-12 GHz. Thus, it can be used to accurately determine the phase for a line having many cascaded sections ($pd_N = N \times pd_1$). Deviations in the linear phase characteristic at the high frequency end result from high radiation and return loss. Shown in figure 5 is the transmission parameter of the line for the same cases. Also given in the inset are the radiation losses. In this example, the line has good transmission below 13 GHz, but the performance deteriorates rapidly after that. Furthermore, at high frequencies, the transmission through the line decreases while the radiation loss increases with line length. From these observations, in addition to acting as a delay line, the meander line is particularly well suited for filtering applications. This is true because the spacing and number of periods control the pass-band corner frequencies and slopes, respectively. This is a well known characteristic of periodic structures in general[24],[25].

Shown in Figures 6 and 7, our theoretical results are compared to theoretical results and experimental data derived by Jansen [21],[22] for shielded and open meander lines, respectively. There is good agreement between the open experimental results and our simulation. This structure has two pass-bands over the frequency range shown. Radiation losses are quite severe and result in degradation of the transmitted power in the 13-20 GHz stopband, and the pencil-thin passband centered at 22.5 GHz. In particular, notice the difference at 22.5 GHz between the

open and shielded simulations. This example illustrates that meander lines may be useful for narrowband applications in monolithic arrays, but they must be designed carefully to avoid unacceptable radiation losses.

4 Junctions

Transmission line junctions are found in virtually every type of microstrip layout and are integral parts of power splitters, matching networks, and couplers. Consequently, a thorough understanding of their parasitic behavior is crucial in high frequency (M)MIC design.

Figure 8 displays the network parameters for mitered and right-angle bend discontiuities. The mitered case has superior behavior as illustrated by its improved return loss. Nonetheless, it is interesting to note that the two structures exhibit almost identical radiation properties (as shown in the inset). It was found that the mitering, in this case, sharply lowers the return loss by decreasing the excess capacitance of the bend, but has little effect on radiation losses. For further improvement in performance, a multiple layer substrate may be utilized to lower radiation loss[6].

Following the method described previously, network parameters have been extracted for three-port T-junction and four-port cross junction discontinuities, with interesting results. As shown in Figure 9, the magnitude of the S-parameters of a T-junction on a 25 mil duroid ($\epsilon_r = 2.2$) substrate agree well with available CAD results[26]. On the the other hand, as shown in figures 10 and 11 for cross and T-junctions respectively, the phase can disagree appreciably with those predicted

by commercial CAD, particularly between ports at right angles. The disagreement arises because of the radiation loss shown in Figure 12 which, although not severe, can have a large effect on the phase of the transmission parameters.

Also shown in Figure 12 are the radiation losses of a right-angle bend having the same strip width and printed on the same substrate. The three types (right-angle bend, cross, and tee) of junctions exhibit similar radiation losses. The lowest loss corresponds to the cross junction which is the only one of the three not having a port current terminate at an edge.

5 Stubs

Open circuit stubs are often used in microstrip matching networks, particularly in (M)MIC amplifiers. Radiation loss and spurious coupling from a matching network have a direct impact on the noise performance of an amplifier and must therefore be minimized. Several stub geometries have been proposed for enhancing various circuit characteristics including reduced loss. The fullwave analysis presented has been employed to evaluate three types of stubs: a)rectangular, b)radial, and c) triangular in terms of their bandwidth, resonance characteristics, and radiation properties. The stubs are printed on a 25 mil GaAs substrate ($\epsilon_r = 12$), and have dimensions shown in Figure 14. For comparison purposes, all of the stubs are designed to have first resonance at about 24 GHz. Two-port scattering parameters have been obtained by positioning the stubs shuntly across a transmission line, as shown. At resonance, the magnitude of the transmission parameter reaches a minimum. Due to radiation loss, which may be viewed as a radiation resistance at

the junction, this minimum is not zero as it would be in the lossless case. Figure 13 shows the transmission parameters for the three cases from 15 to 28 GHz. As shown, the radial stub has the broadest bandwidth, and the triangular stub has the narrowest. These results indicate that the bandwidth may be adjusted by varying the angle of the radial stub. However, it should be noted that such a modification will also shift the resonant frequency.

As previously mentioned, radiation from matching networks has a direct and derogatory effect on noise performance in (M)MIC amplifiers. Figure 14 shows quite clearly that the triangular shape radiates more than the other two types. Additionally, the radial stub shows moderate improvement over the rectangular type. The loss peaks for all three cases at 27 GHz (about 3-4 GHz beyond resonance), indicating that the radiation properties are heavily influenced by the characteristics of the substrate. For the given substrate at this operating frequency, the loss is primarily due to the TM_0 substrate mode. We conclude that since the triangular stub has the smallest bandwidth, and radiates most severely, it is only recommended for narrowband, low loss applications. The rectangular and radial stubs have similar radiation properties, with the radial stub having a broader band response.

5.1 Matching Circuit for 94 GHz Oscillator

Figure 16a shows a matching circuit for a submillimeter wave oscillator designed to operate at 94 GHz. The network is printed on 100 μm GaAs ($\epsilon_r = 12.8$). The analysis was applied to obtain scattering parameters individually for the cross junction stub (stub A), the T-junction stub (Stub B), and the entire matching

section. The results presented in this section are normalized to fifty ohms. Of interest in this analysis are the radiation losses experienced as the stubs pass through a quarter wave resonance, and the coupling between the two stubs. Frequently, such a design would be done with available CAD by individually modeling the two stubs, and then chaining together the S-parameters. Therefore, electromagnetic interactions between the stubs would not be included. For this case, the coupling will be shown to be significant, because the stubs are in close proximity and have approximately the same resonant frequency.

Shown in Figures 15(a) and (b) are the scattering parameters for the cross junction and the T-junction stub, respectively. The quarter wave resonance of the stubs are 145 GHz for stub A and 160 GHz for stub B as determined by the minima in the magnitude of S12. There is appreciable radiation loss beyond the resonances of the two stubs. This radiation causes a degradation in the magnitude of S11 at the high frequency end of the simulations for both stubs. The T-junction stub, having twice the thickness of the cross-junction stub, radiates more power. In fact, as shown in Figure 17, at 200 GHz it is radiating almost half of its input power.

The scattering parameters for the entire matching network are shown in Figure 16 (b). At the lower frequency ranges (below 140 GHz), the radiation losses are not significant. Thus, the network should function adequately at the oscillation frequency. In this example, although the $100\mu m$ substrate is physically thin for present technology, it becomes electrically thick at higher frequencies (one-fifth of a wavelength in the dielectric at 170 GHz), and high radiation losses are encountered.

as shown in Figure 17. This result illustrates the difficulty with using microstrip circuits at sub-millimeterwave frequencies.

The entire matching network radiates less than Stub B alone. At first glance this appears anomalous, but it is a result of electromagnetic coupling between the stubs. The spacing of the stubs is approximately one half wavelength at the upper frequencies. Therefore, the stubs are radiating 180 degrees out of phase, and phase cancellation is occurring in the radiated fields. This example indicates that, under the right conditions, electromagnetic coupling between adjacent stubs can impact performance.

6 Conclusion

The high frequency behavior of a wide range of open microstrip elements has been presented. Results were obtained by the space domain integral equation approach which includes all electromagnetic coupling and radiation effects. In addition, resistive loss was included through the replacement of the microstrip conducting strips by the appropriate surface impedance boundary. This results in, for the first time, a unified analysis accounting for both resistive and radiation loss. The previous sections included examples of microstrip meander lines, bends, multi-port junctions, and tuning stubs.

Two applications of meander lines were shown. First, the effect of radiation and conductor losses on meander line phase shifting sections were presented. These loss mechanisms were shown to reduce the transmission through the line at higher frequencies and longer lengths. Also, an example was given which demonstrated

that a long meander line can be accurately characterized by a single one of its periods. The second application demonstrates the meander line's filter properties with an example exhibiting a very narrow pass-band.

Scattering parameters and radiation losses for several microstrip junctions were presented. The favorable effect of mitering on the return loss for a bend discontinuity was demonstrated. Furthermore, it was shown that bend, cross, and tee junctions printed on a common substrate with the same linewidth exhibited similar radiation properties.

In the final section, three stub geometries, rectangular, radial, and triangular, were investigated. The radial stub was shown to have the broadest bandwidth of the three with comparable radiation properties to the rectangular stub. The triangular stub had the most narrow bandwidth, and the most severe radiation loss.

The final example given was a matching circuit for a submillimeter wave HEMT oscillator. This example demonstrated that electromagnetic coupling between stubs in close proximity can have a significant influence on circuit performance.

MISSING PAGE

References

[1] P.B. Katehi and N. G. Alexopoulos, "Frequency-Dependent Characteristics of Microstrip Discontinuities in Millimeter-Wave Integrated Circuits",*IEEE Trans. Microwave Theory Tech.*, Vol. MTT-33, Oct. 85, pp. 1029-1035.

[2] R. W. Jackson, and D. M. Pozar, "Full-Wave Analysis of Microstrip Open-End and Gap Discontinuities",*IEEE Trans. Microwave Theory Tech.*, Vol. MTT-33,Oct. 85, pp. 1036-1042.

[3] N. G. Alexopoulos, P.B. Katehi, and D. Rutledge, "Substrate Optimization for Integrated Circuit Applications," *IEEE Trans. Microwave Theory Tech.*, Vol. MTT-31, pp. 550-557, July, 1983.

[4] R. Jackson, "Full-Wave Finite Element Analysis of Irregular Microstrip Discontinuities, *IEEE Trans. Microwave Theory Tech.*, Vol. MTT-37, pp. 81-89, Jan. 89.

[5] J. R. Mosig, "Arbitrarily shaped microstrip structures and their analysis with a mixed potential integral equation, *IEEE Trans. Microwave Theory Tech.*, Vol. MTT-36, pp. 314-323, Feb. 1988.

[6] W. P. Harokopus, Jr. and P. B. Katehi, "An Accurate Characterization of Open Microstrip Discontinuities Including Radiation Losses",*IEEE Trans. Microwave Theory Tech.*, Vol. MTT-37, Dec. 89, pp. 1964-1972.

[7] M. Maeda, "Analysis of Gap in Microstrip Transmission Lines", *IEEE Trans. Microwave Theory Tech.*, Vol. MTT-20, pp.390-396, Jun. 1972.

[8] P. Benedek and P. Silvester, "Equivalent Capacitance of Microstrip Gaps and Steps", *IEEE Trans. Microwave Theory Tech.*, Vol. MTT-20, pp.729-733, Nov. 1972.

[9] P. Silvester and P. Benedek, "Equivalent Capacitance of Microstrip Open Circuits," *IEEE Trans. Microwave Theory Tech.*, Vol. MTT-20, pp. 511-516, Aug. 1972.

[10] P. Silvester and P. Benedek, "Equivalent discontinuities capacitances for Right-Angle Bends, T-junctions, and Crossings," *IEEE Trans. Microwave Theory Tech.*, Vol. MTT-21, pp. 341-346, May 1973.

[11] R. Horton, "The Electrical Characterization of a Right-Angle Bends in Microstrip Line," *IEEE Trans. Microwave Theory Tech.*, Vol. MTT-21, pp.427-429, Jun. 1973.

[12] T. Itoh, "Analysis of Microstrip resonators", *IEEE Trans. Microwave Theory Tech.*, Vol. MTT-22, pp.946-952, Nov. 1974.

[13] I. Wolf, G. Kompa, and R. Mehran, "Calculation Method For Microstrip Discontinuities and T-Junctions," *Electron. Lett.*, Vol. 8, 1972.

[14] G. Kompa, and R. Mehran, "Planar Waveguide Model For Calculating Microstrip Components," *Electron. Lett.*, Vol. 11, 1975.

[15] W. Menzel and I. Wolf, "A Method For Calculating the frequency Dependent Properties of Microstrip Discontinuities," *IEEE Trans. Microwave Theory Tech.*, Vol. MTT-25, pp. 107-112, Feb. 1977.

[16] A. Sommerfeld, Partial Differential Equations in Physics, New York, N.Y., Academic Press, 1949.

[17] R.S. Elliott, "The Green's Function For Electric Dipoles Parallel To and Above or Within a Grounded Dielectric Slab", Hughes Technical Correspondence, 1978.

[18] R. F. Harrington, Field Computation By Moment Methods, Macmillan,N.Y. ,1968.

[19] A.C. Cangellaris, "The Importance of Skin-Effect in Microstrip Lines at High Frequencies",*IEEE MTT-International Symposium Digest*,pp 197-198, May 1988.

[20] T.E. van Deventer, P. B. Katehi, and A. C. Canggellaris, "An Integral Equation Method For The Evaluation of Conductor and Dielectric Losses in High Frequency Interconnects", *IEEE Trans. Microwave Theory Tech.*, Dec. 1989.

[21] W. Wertgen, and R. H. Jansen, "Novel Green's Function Database Technique For Efficient Full-Wave analysis of Complex Irregular (M)MIC-Structures", European Microwave Conference Proceedings, September 1989, pp.199-204.

[22] W. Wertgen, and R. H. Jansen, "Efficient Direct and Iterative Electrodynamic Analysis of Geometrically Complex IrregularMIC and MMIC-Structures", International Journal of Numerical Modelling, September 1989, pp.153-186.

[23] P.S. Hall and S.J. Vetterlein, "Microstrip Patch Array With Multiple beams", European Microwave Conference Proceedings, September 1989, pp. 343-348. *IEEE Trans. Microwave Theory Tech.*, Dec. 1989.

[24] J. A. Weiss, "Dispersion and Field Analysis of a Microstrip Meander-Line Slow-Wave Structure," *IEEE Trans. Microwave Theory Tech.*, Vol. MTT-22, No. 12, pp. 1194-1201.

[25] V. Rizzoli, and A. Lipparini, "Bloch-Wave Analysis of Stripline- and Microstrip-Array Slow-Wave Structures," *IEEE Trans. Microwave Theory Tech.*, Vol. MTT-29, No. 29, pp. 143-149.

[26] EESOF, *Touchstone*, EESOF INC., Westlake Village, CA. 91362.

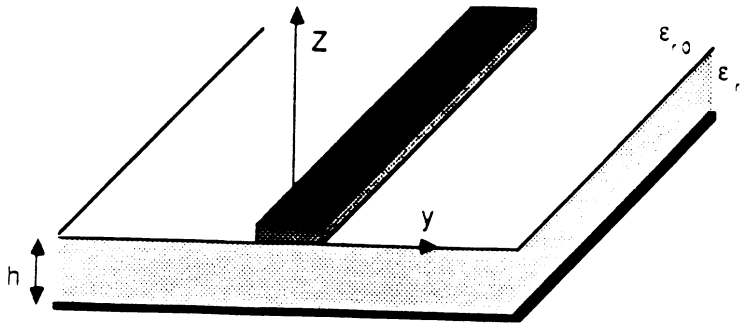

a. Cross-Sectional View

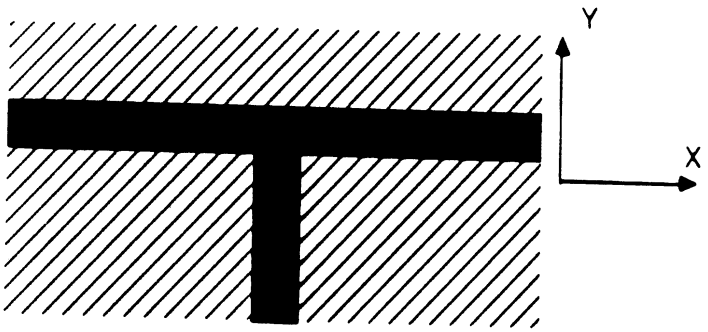

b. Top View

Figure 1: Open Microstrip Geometry

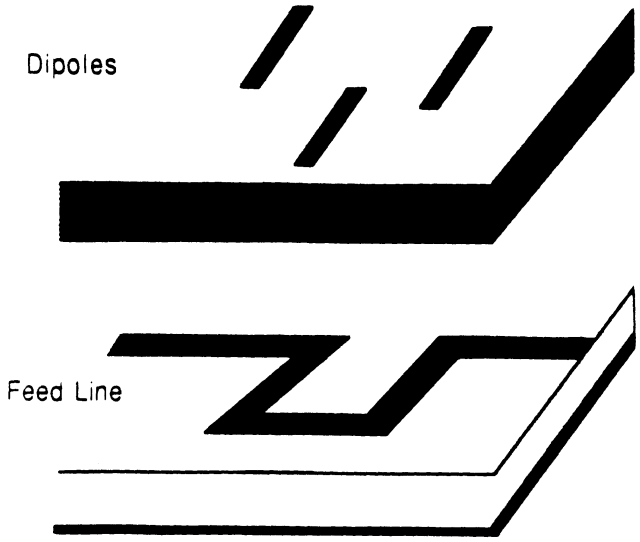

a. Cross-Sectional View

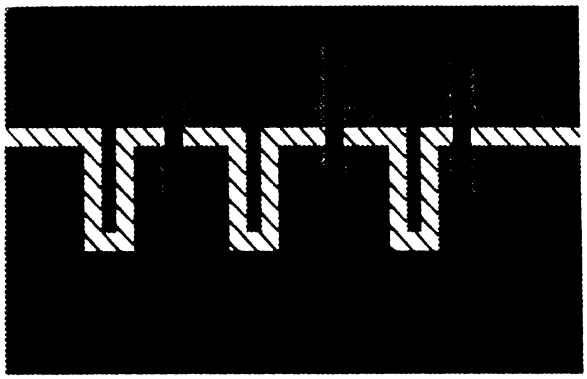

b. Top View

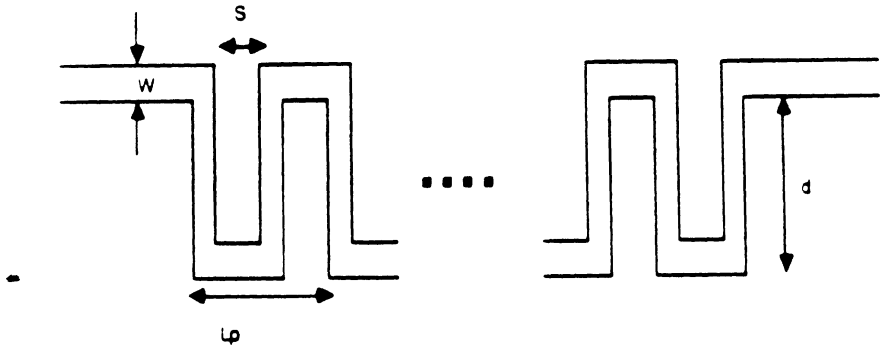

c. Meander Line Parameters

Figure 2: Microstrip Meander Line Feeding Dipoles

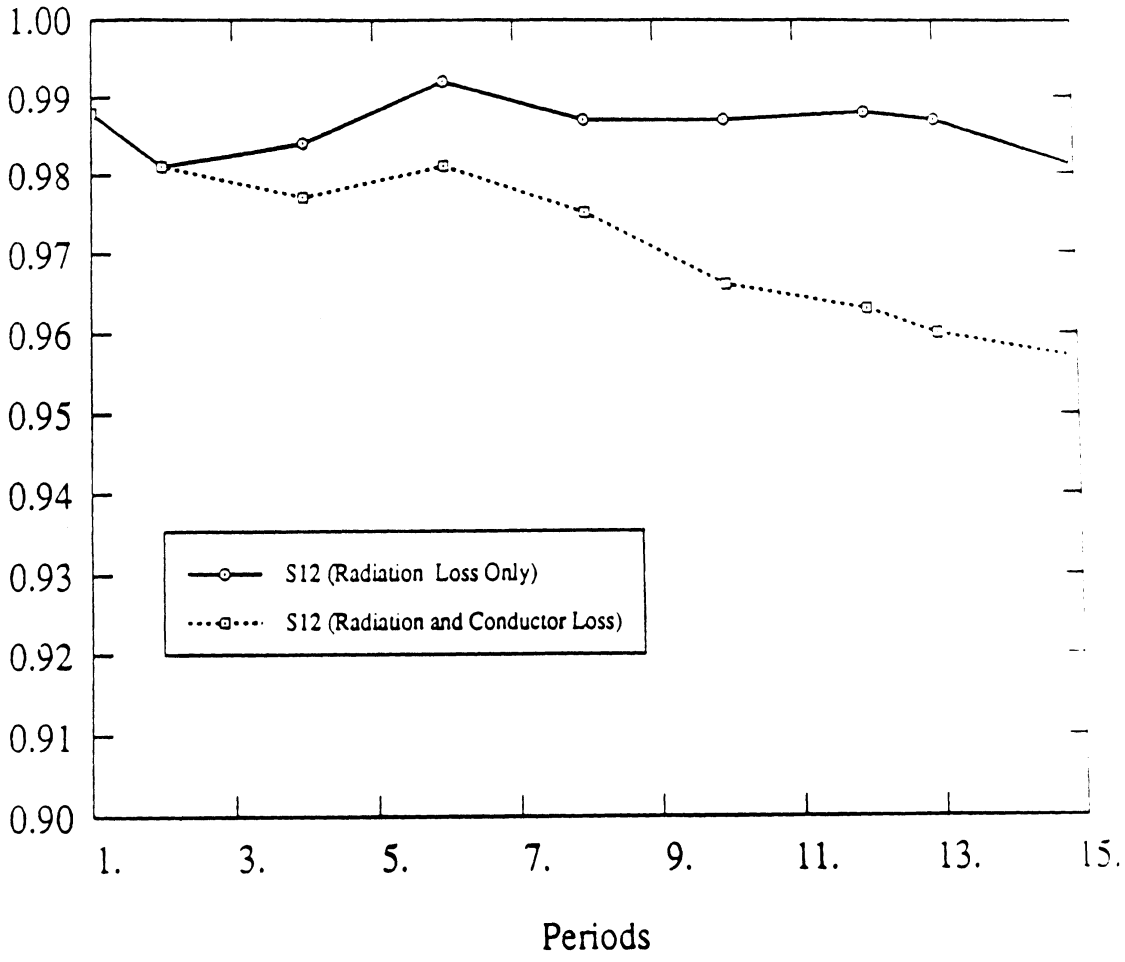

Figure 3. Transmission parameter magnitude of meander line as a function of length (f = $20GHz, \epsilon_r = 2.2, h = 20mil, W = 10mil, S = 10mil, d = 50mil, t = 12\mu m, \sigma = 4x10^7 mmho/m$)

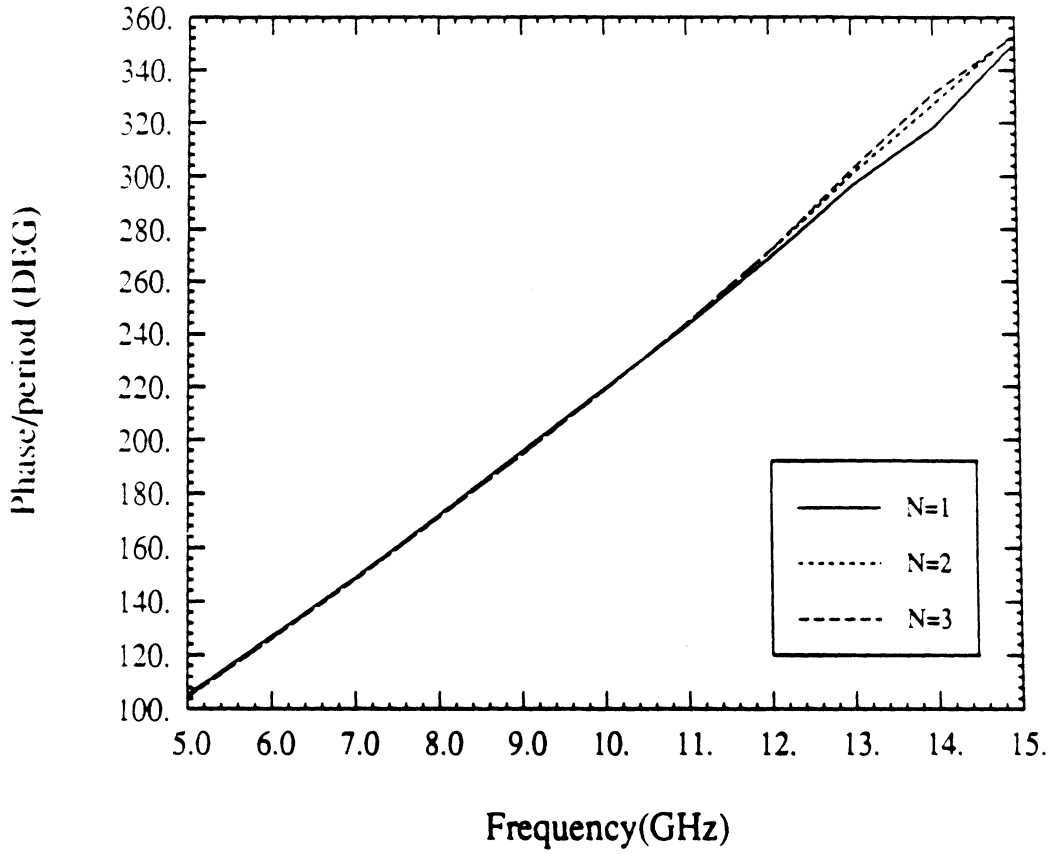

Figure 1: Phase of transmission parameter for meander line as a function of frequency (ϵ_r = 9.978, $h = 25mil$, $W = .305mm$, $S = 4W$, $d = 5W$)

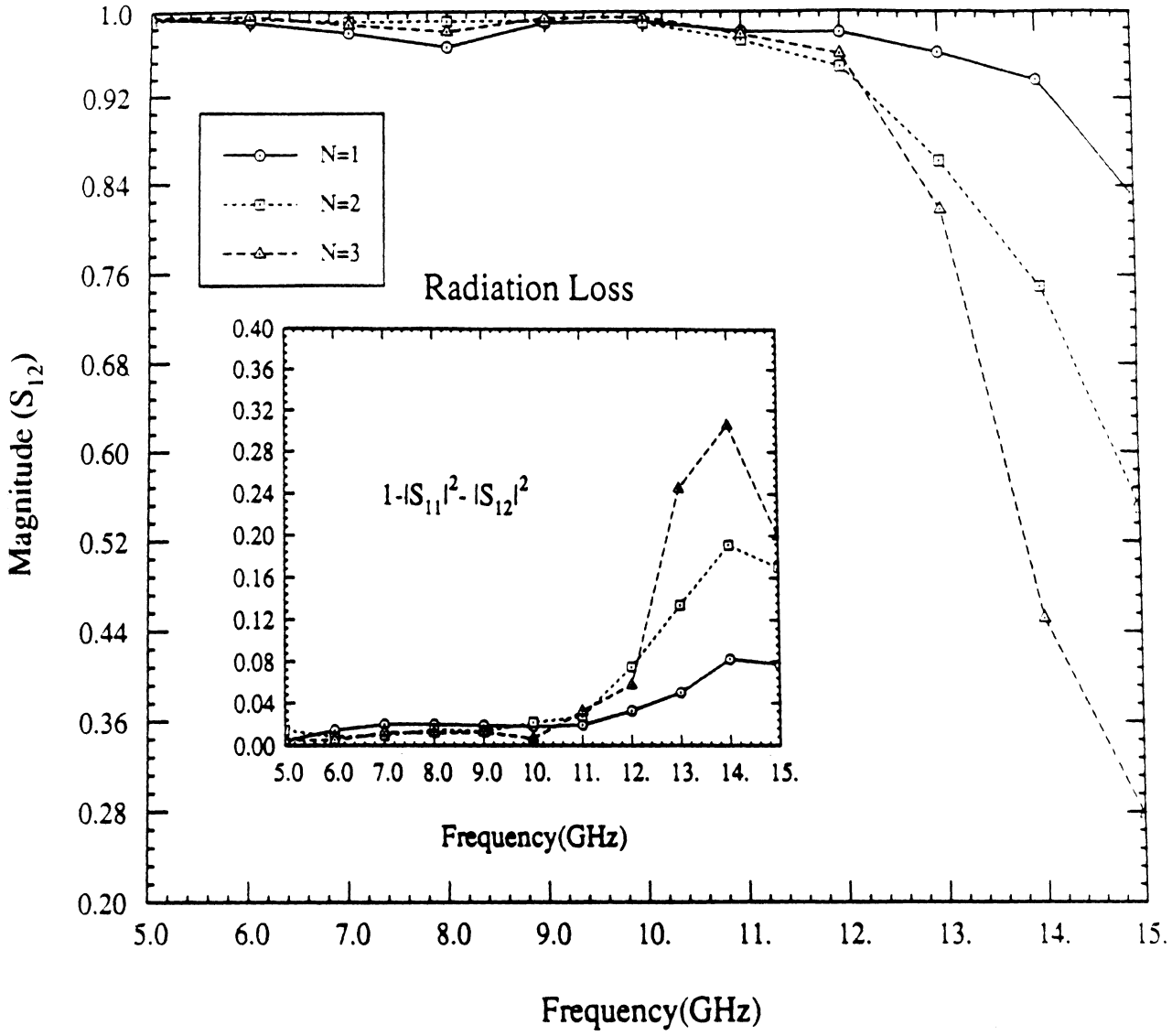

Figure 5 Magnitude of transmission parameter for meander line as a function of frequency ($\varepsilon_r = 9.978$, $h = 25mil$, $W = 305mm$, $S = 4W$, $d = 5W$)

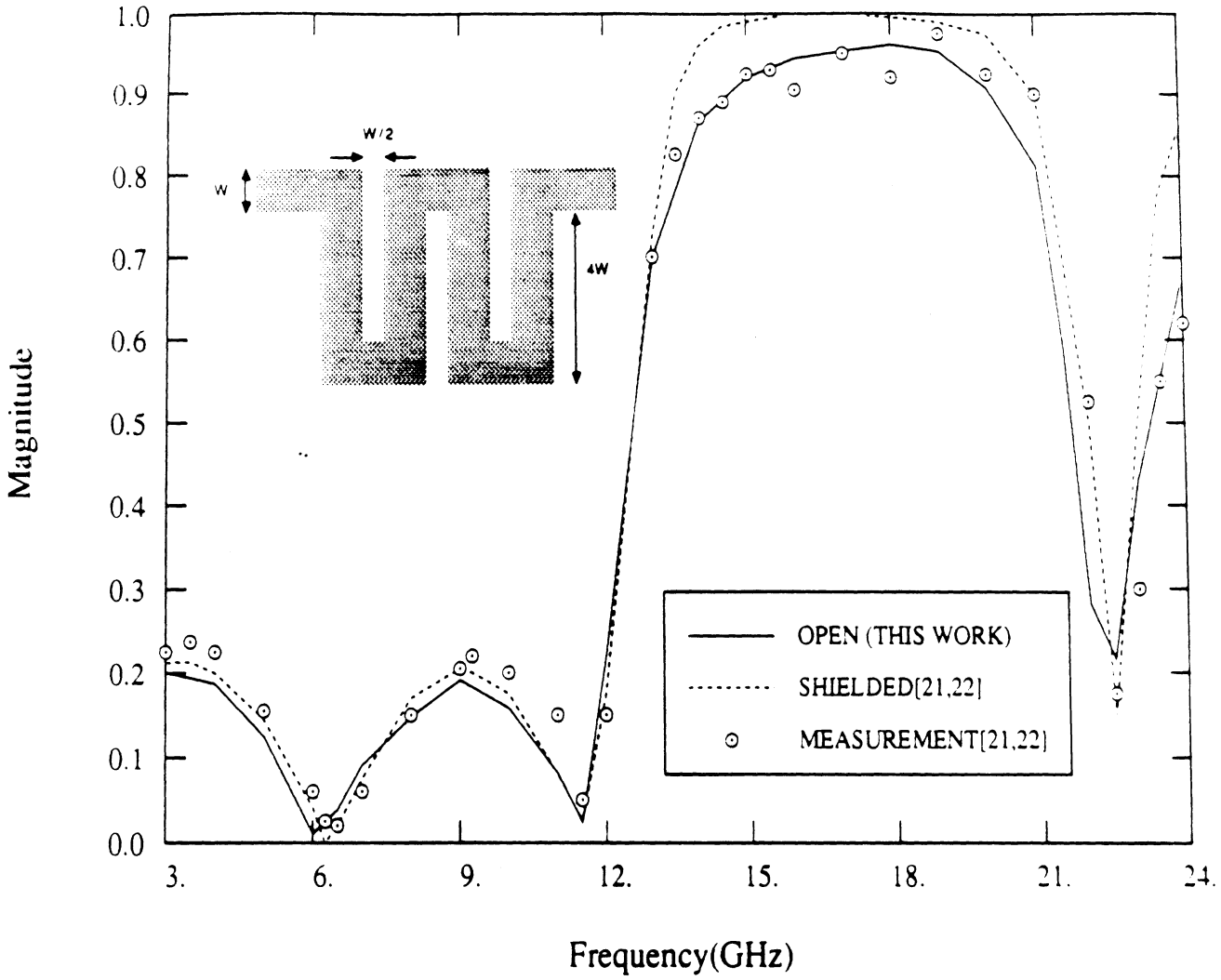

Figure 6. Magnitude of Reflection Coefficient for meander line filter as a function of frequency ($\epsilon_r = 9.978, h = 25mil, W = 61mm, S = \frac{1}{2}W, d = 4W$)

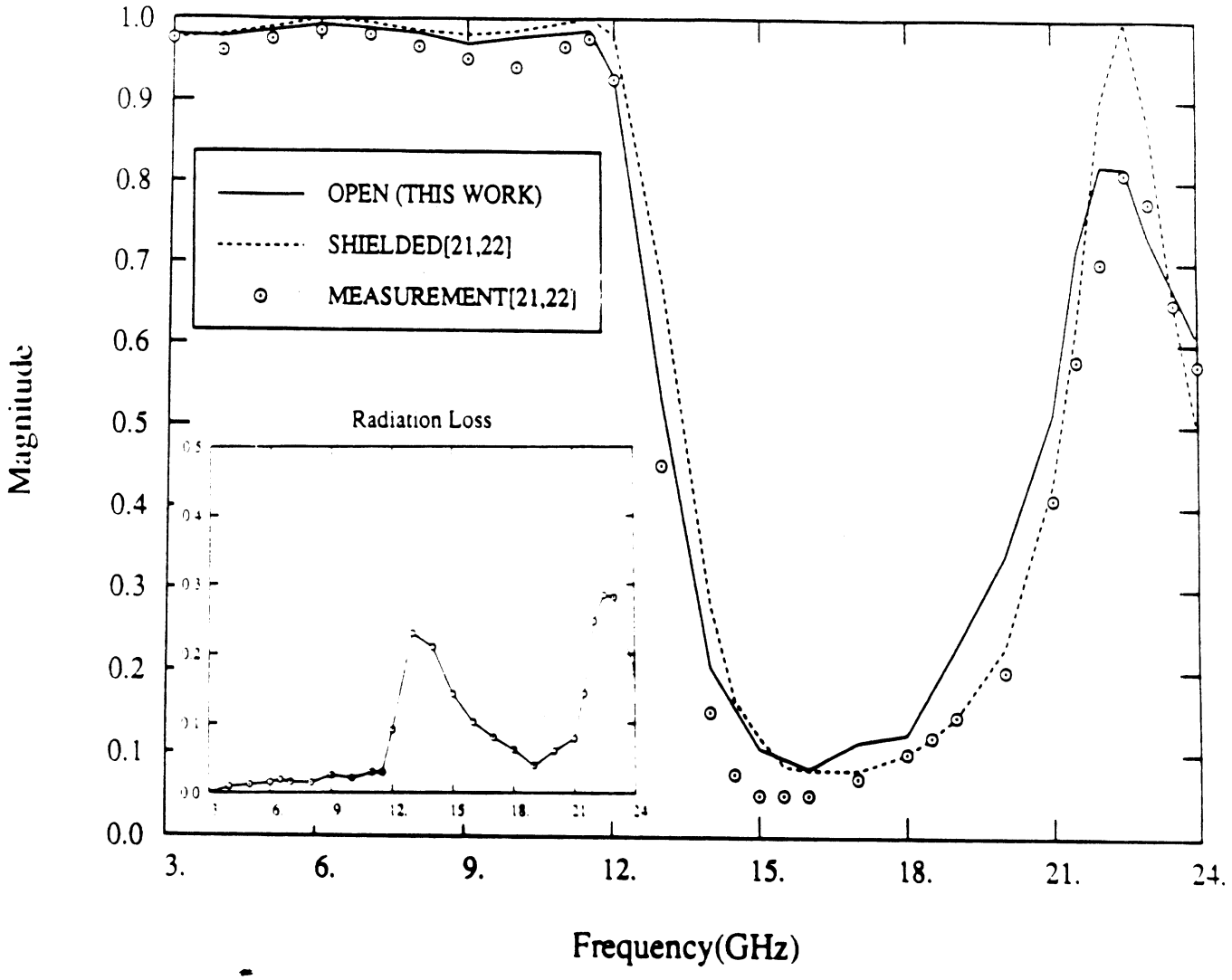

Figure 7. Magnitude of Transmission Parameter for meander line filter as a function of frequency ($\epsilon_r = 9.978, h = 25mil, W = 61mm, S = \frac{1}{2}W, d = 4W$)

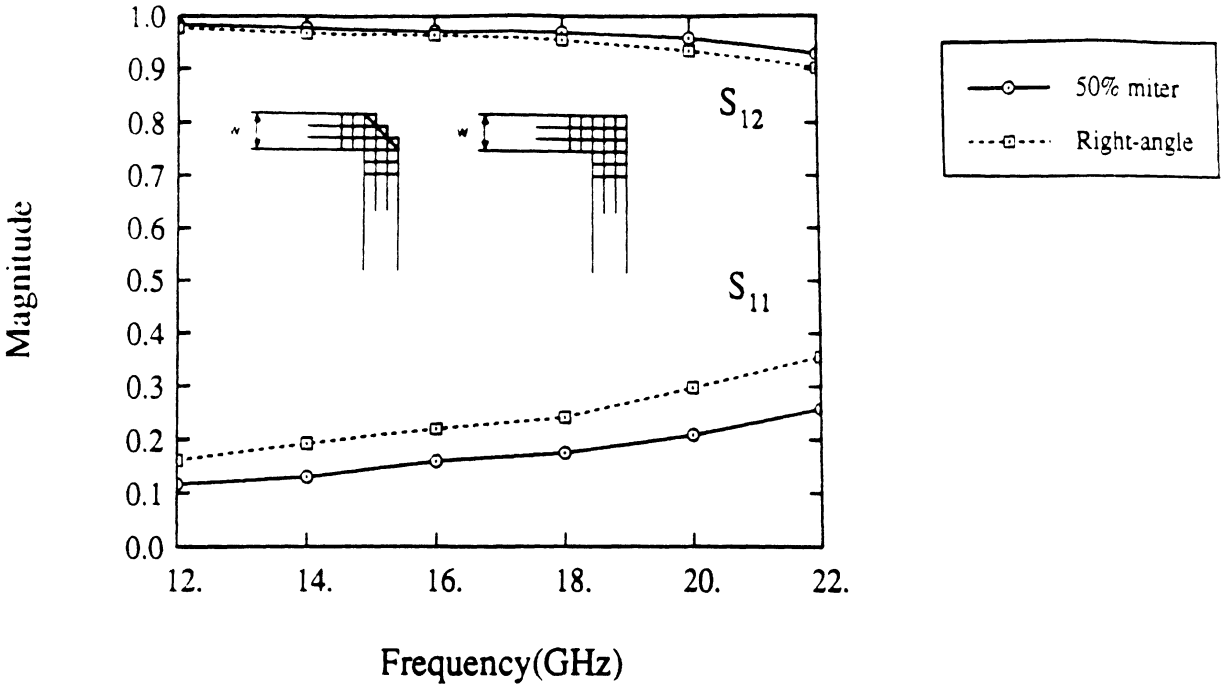

a. Scattering Parameters

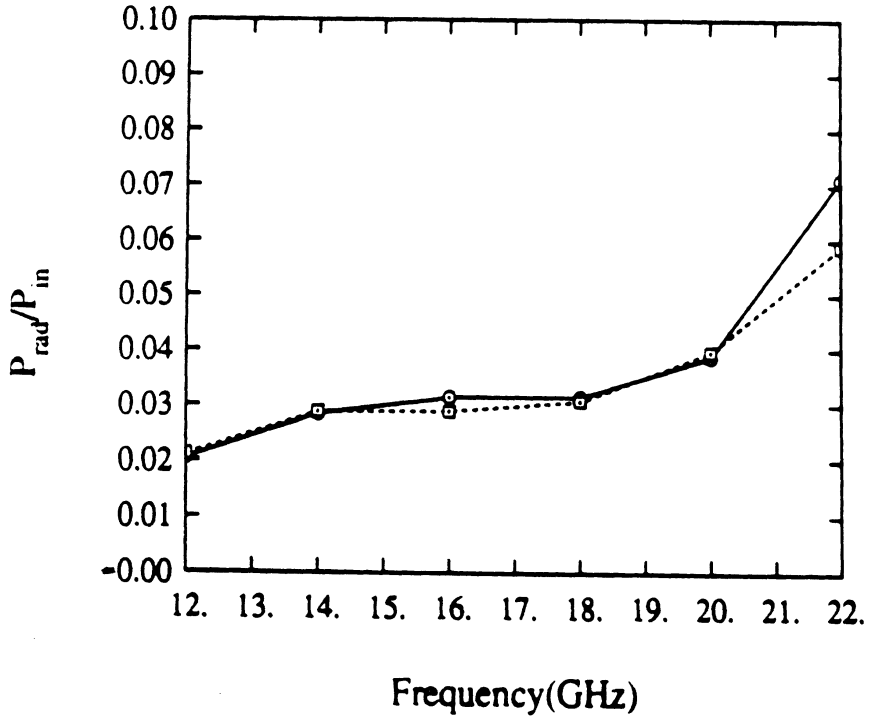

b. Radiation Loss

Figure 8 Network Parameters(magnitude) for right-angle and mitered bends (ϵ_r = 12, h = 25mil, W = 15mil)

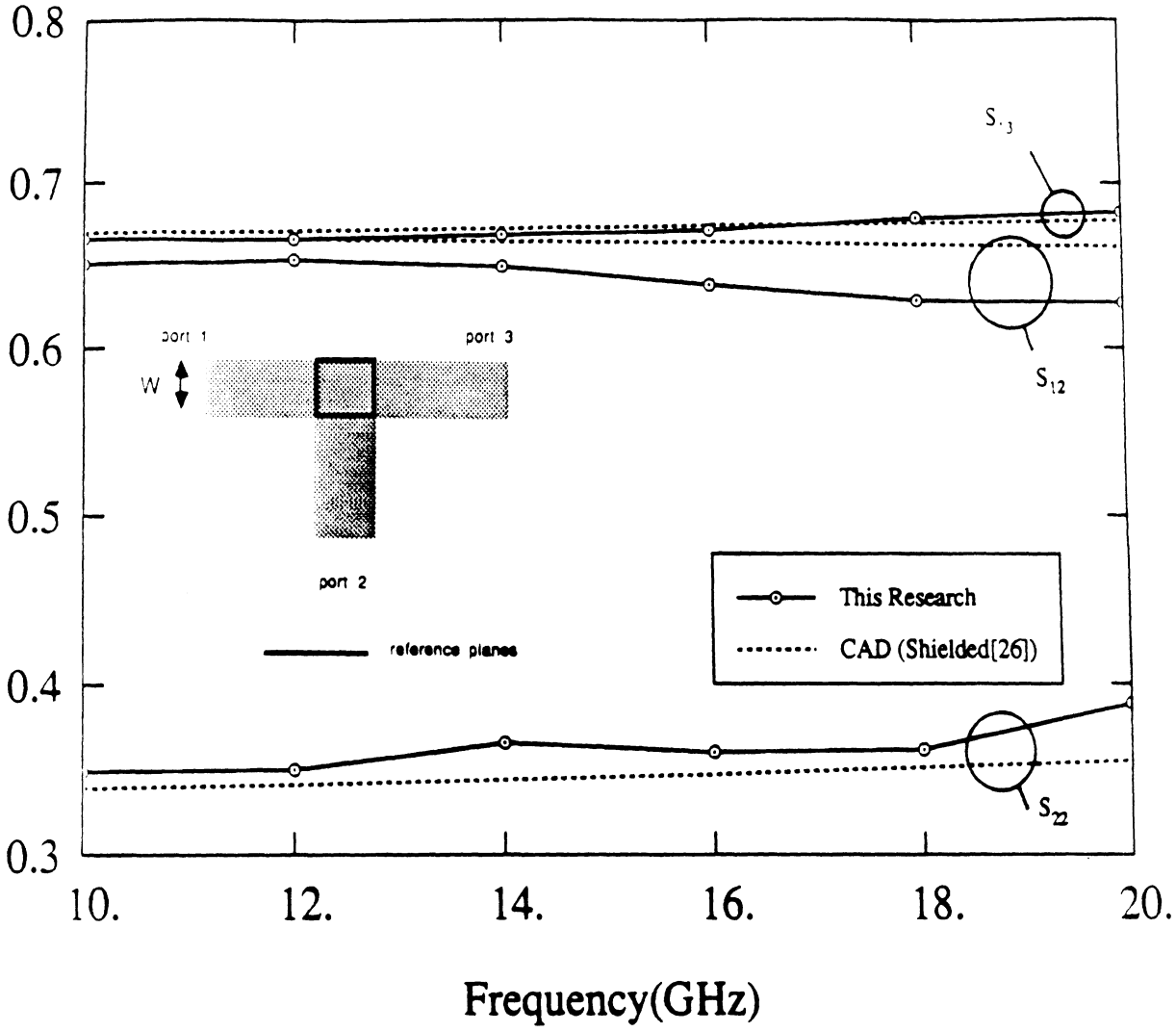

Figure 9: Scattering Parameters(magnitude) for microstrip T-junction as a function of frequency ($\epsilon_r = 2.2, h = 25mil, W = 25mil$)

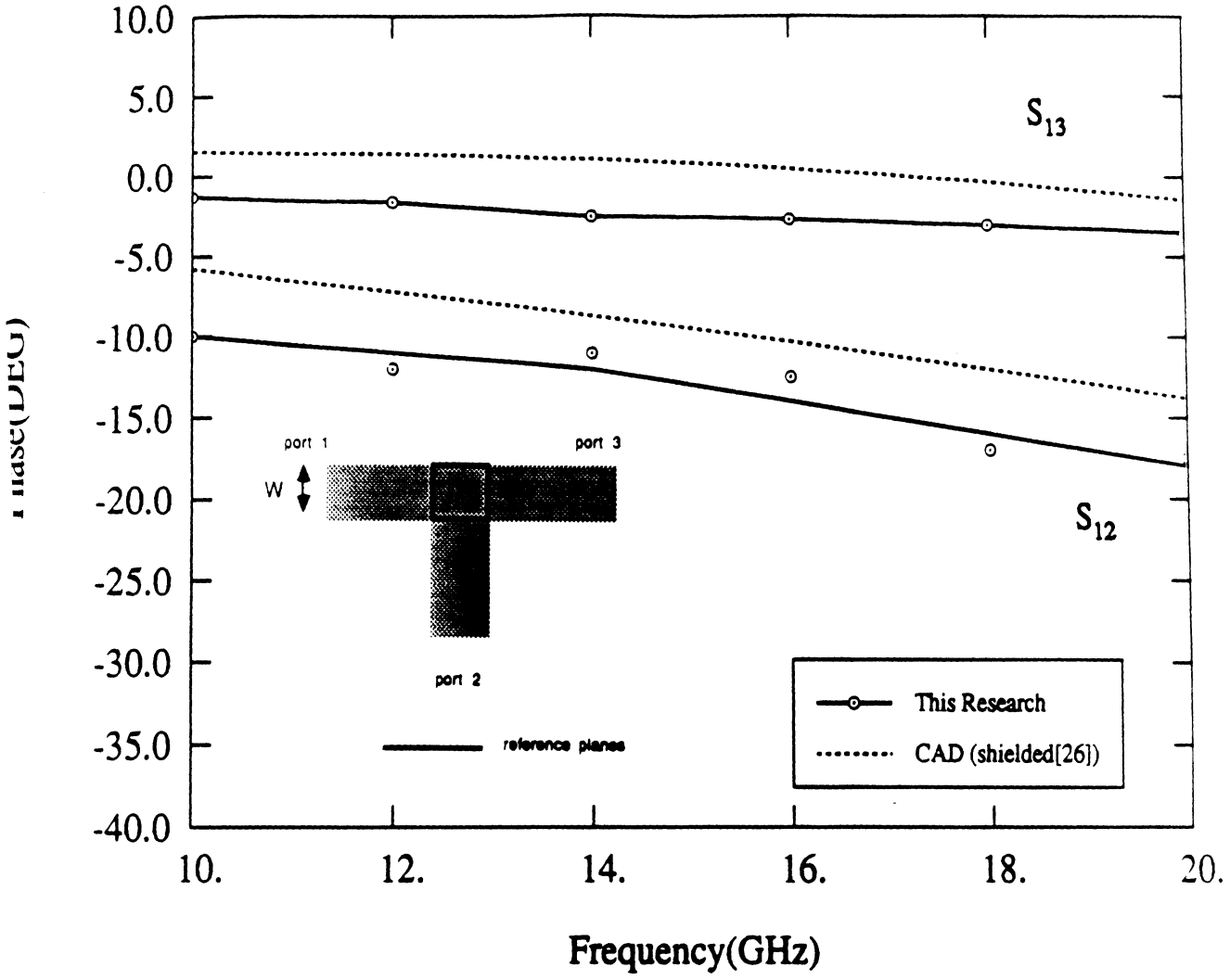

Figure 10: Scattering Parameters(phase) for microstrip T-junction as a function of frequency ($\epsilon_r = 2.2, h = 25mil, W = 25mil$)

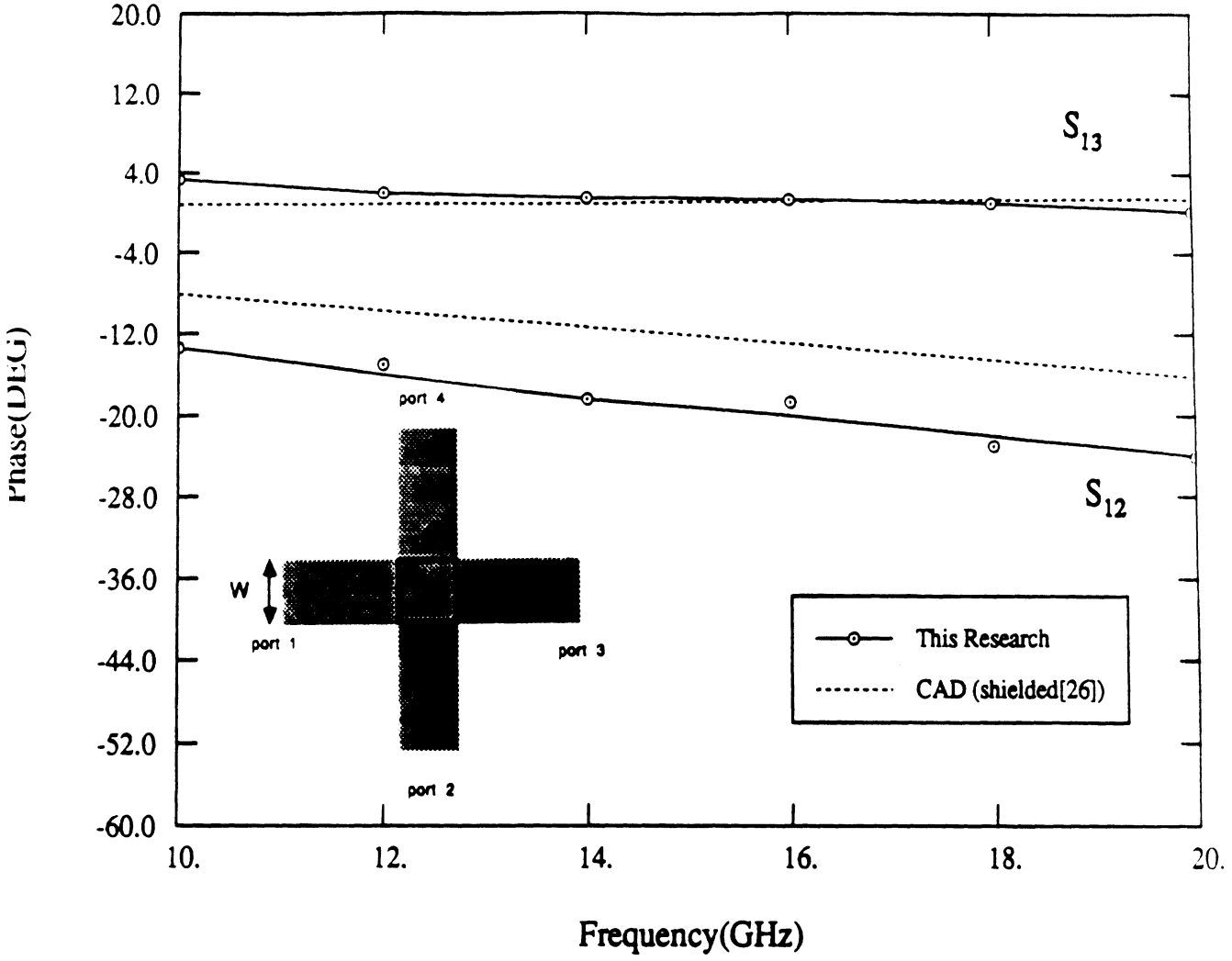

Figure 11: Scattering Parameters(phase) for microstrip cross junction as a function of frequency ($\epsilon_r = 2.2, h = 25mil, W = 25mil$)

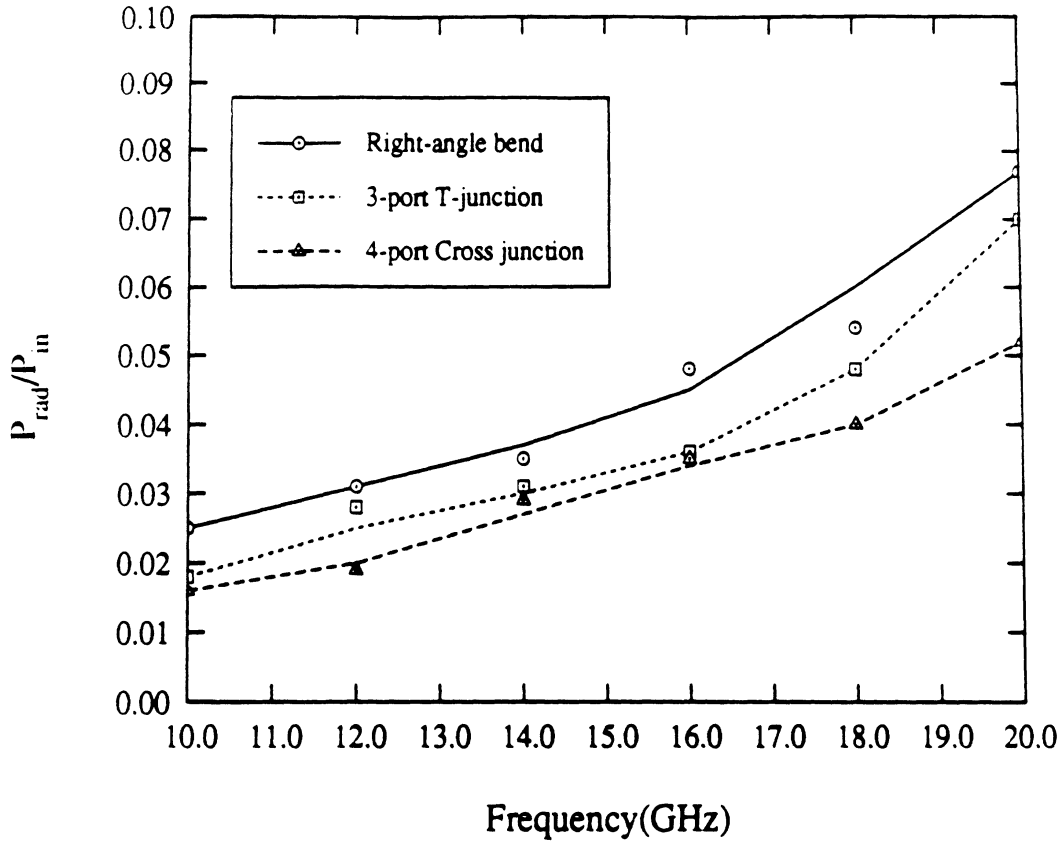

Figure 12: Radiation Loss in microstrip junctions (bend,cross,tee) ($\epsilon_r = 2.2, h = 25mil, W = 25mil$)

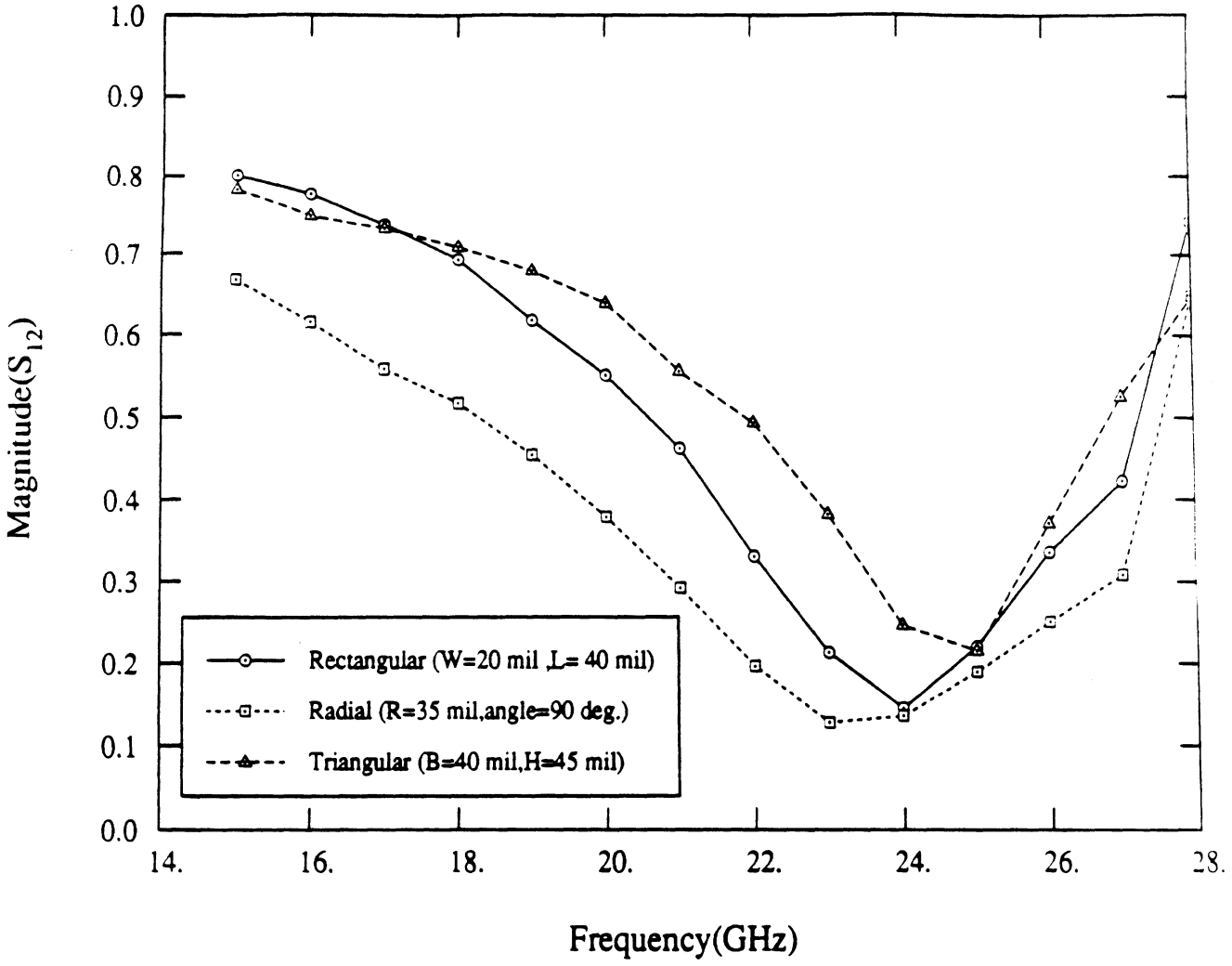

Figure 13: Transmission parameter of microstrip stubs ($\epsilon_r = 12, h = 25mil$)

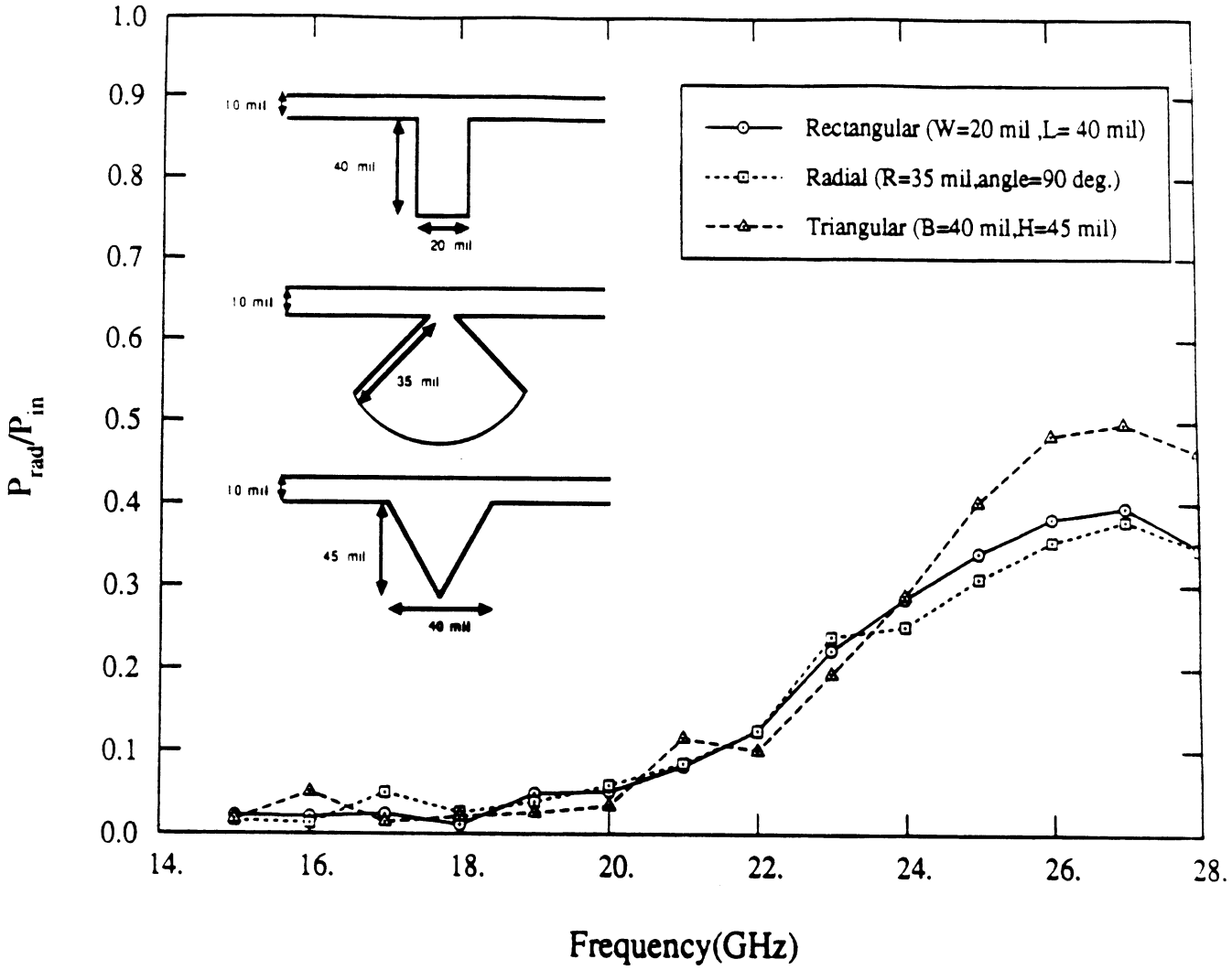

Figure 14: Radiation Loss of microstrip stubs ($\epsilon_r = 12, h = 25mil$)

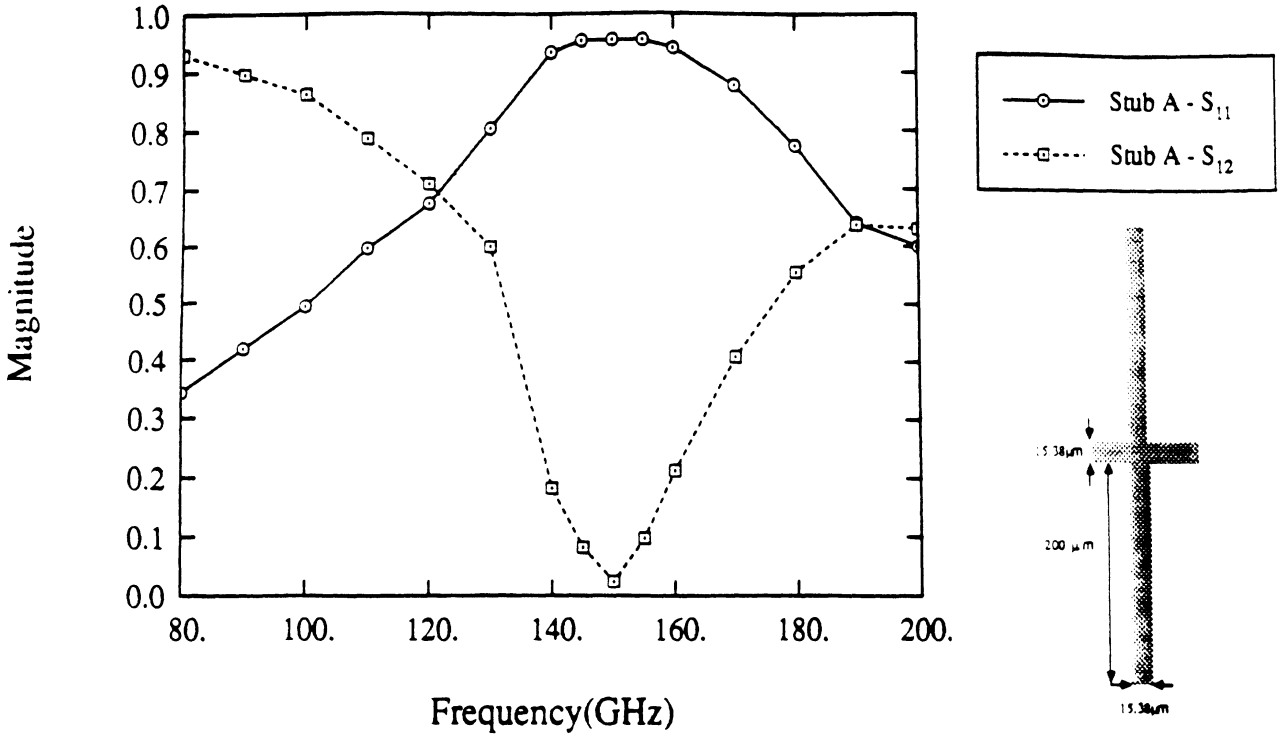

a. Scattering parameters of stub A

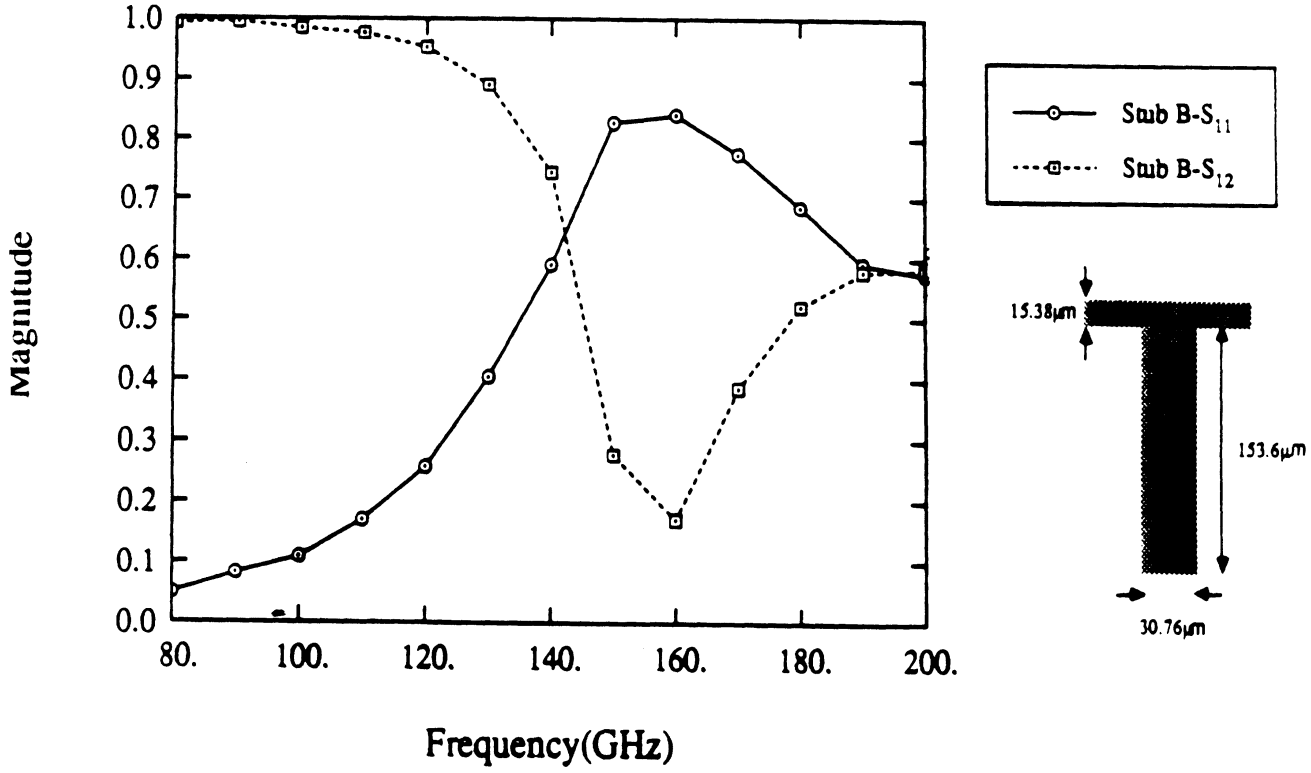

b. Scattering parameters of stub B

Figure 15: Scattering parameters of individual stubs found in oscillator matching circuit (ϵ_r = 12.8, h = 100μm, W = 15.38μm)

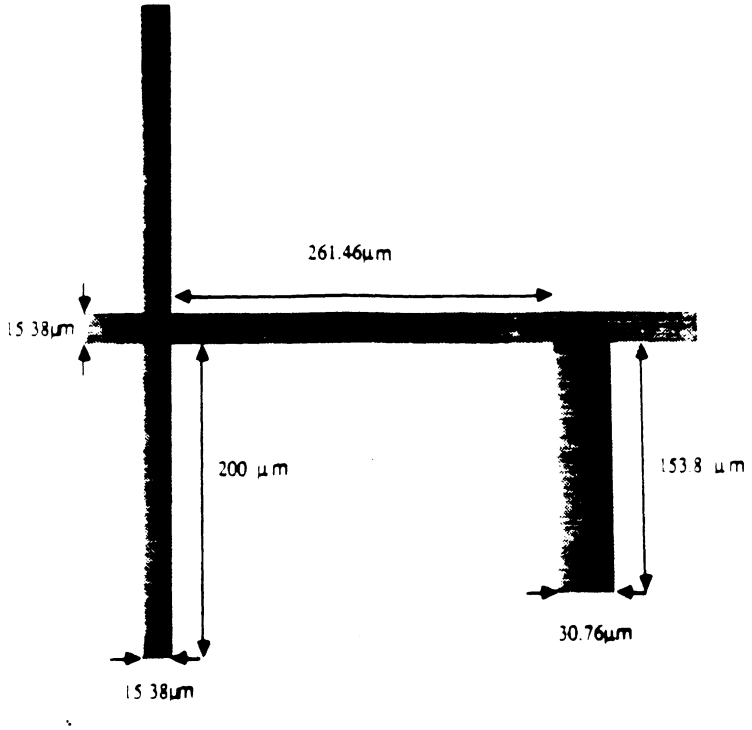

a. Oscillator matching network

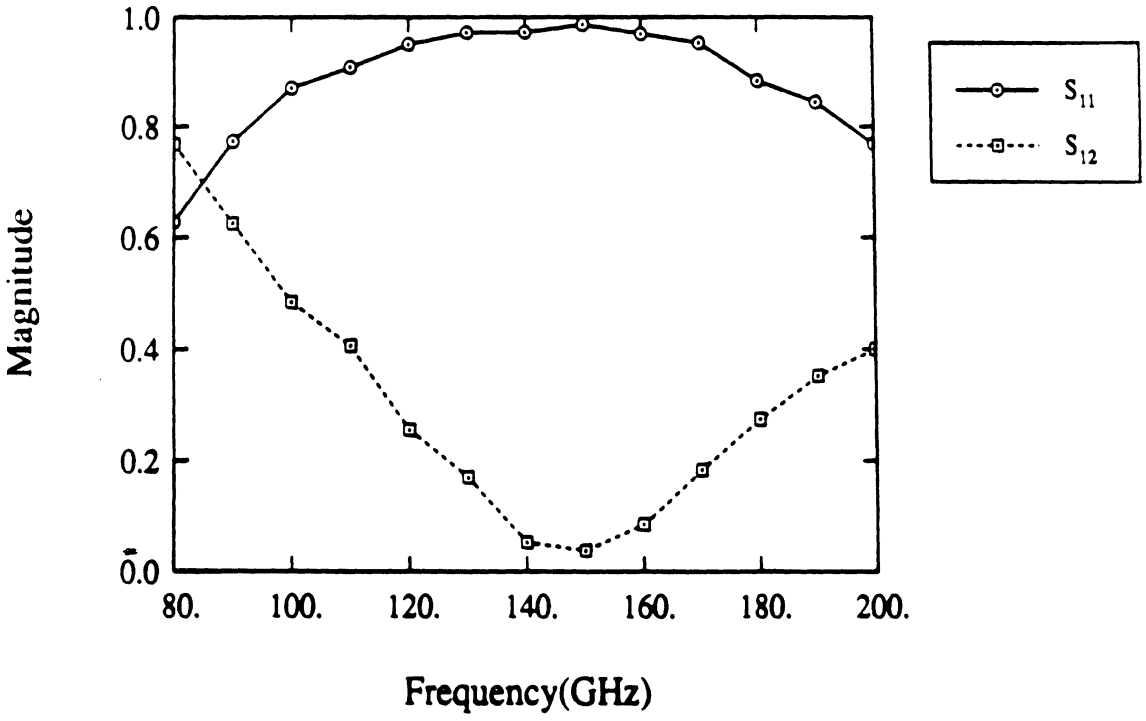

b. Scattering parameters

Figure 16: Scattering parameters of microstrip matching network ($\epsilon_r = 12.8, h = 100\mu m, W = 15.38\mu m$)

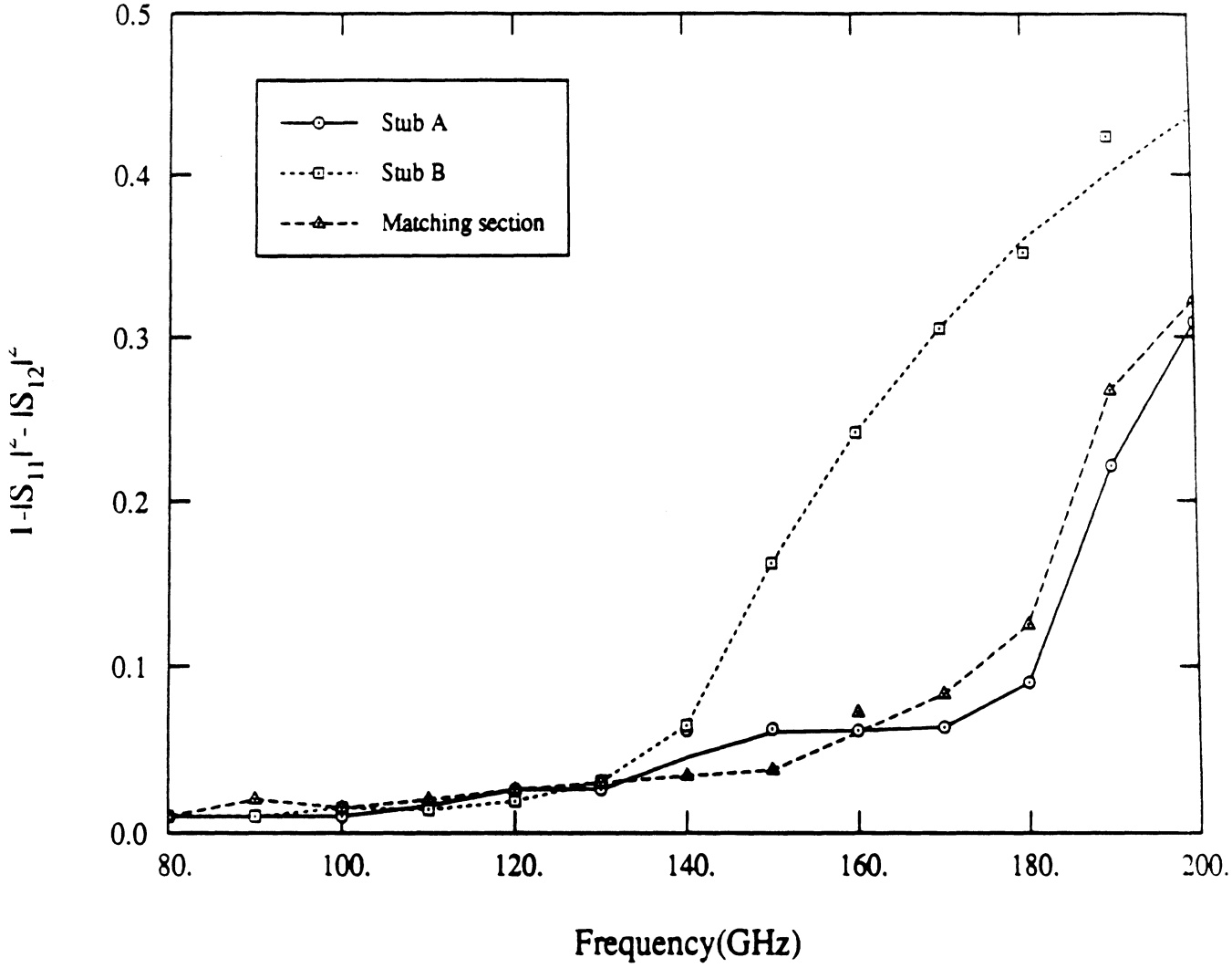

Figure 17: Radiation loss in microstrip matching network ($\epsilon_r = 12.8, h = 100\mu m, W = 15.38\mu m$)